Renewable Energy 224 (2024) 120154

Contents lists available at ScienceDirect

Renewable Energy

journal homepage: www.elsevier.com/locate/renene

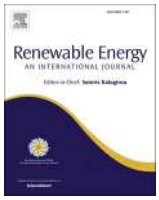

Solar to hydrogen conversion by a 25 cm^2-photoelectrochemical cell with upscaled components

O. Barbera [a,*], C. Lo Vecchio [a], S. Trocino [a], A. Carbone [a], A.S. Aricò [a], V. Baglio [a], G. Giacoppo [a,**]

[a] *Institute for Advanced Energy Technologies "Nicola Giordano" - CNR-ITAE, Via Salita S. Lucia sopra Contesse 5 - 98126 Messina, Italy*

ARTICLE INFO

Keywords:
Photoelectrochemical tandem cell
Hydrogen production
Hematite photoanode
Anion exchange membrane
Copper oxide photocathode
Cell prototype

ABSTRACT

An innovative tandem photoelectrochemical cell with a scaled-up active area from 0.25 to 25 cm^2 based on low-cost and non-critical raw materials was employed to produce green hydrogen by water splitting. It uses a photoanode/membrane/photocathode tandem cell configuration in which a hematite-based photoanode is layered on a fluorine-doped tin oxide glass for the oxygen evolution reaction, CuO is deposited on a hydrophobic gas diffusion layer as the photocathode for the hydrogen evolution reaction and an anion exchange membrane is used as the electrolyte and gas separator. The solid membrane's low hydrogen and oxygen crossover guarantees the operational stability of the tandem photoelectrochemical cell and the efficient separation of water-splitting products. Significant efforts have been focused on scaling up the cell. It has allowed obtaining, for the first time, a 25 cm^2 unit cell prototype. Appropriate design approaches have been considered to optimise water/gas management, current collection, gas-tightness and clamping. The adopted architecture allowed for the reduction of the bias-potential from −1.23 V, generally employed to investigate PEC cells, up to −0.6/-0.4 V 20 h-durability tests demonstrated good resistance to corrosion, showing a constant photocurrent. Efficiency at −0.6 V was about 0.2%. Selective hydrogen production was demonstrated by mass spectrometric analysis.

1. Introduction

Nowadays, fossil fuels cover most of the world's energy demand. These fuels supply the energy for industry, residential applications, and transportation sectors [1–3]. However, these resources are not sustainable in the long term and cause climate change issues such as global warming through greenhouse gas emissions. So, there is an increasing interest in the future role of renewable energy sources, which could become an attractive alternative to fossil fuel-based ones. It is also aided by the continuous decrease in the cost of wind and solar energy as opposed to the rising price of fossil fuels [4,5].

Nevertheless, a well-known problem with most renewable energy sources is the intermittence of their power production that the existing grid cannot easily tolerate. In this regard, hydrogen is considered an energy carrier, which can become the primary approach for alternative energy storage [6,7]. Indeed, it can be converted into electrical energy using fuel cells, fed into natural gas pipelines, and used as a fuel for turbines and internal combustion engines. Among the numerous proposed methods, photoelectrochemical (PEC) water splitting (WS) from sunlight is considered the most promising process for green hydrogen production [8–10]. A PEC cell uses electricity directly converted from sunlight to implement WS; it comprises two electrodes immersed in an aqueous electrolyte or separated by a hydrated solid electrolyte, at least one of which consists of a semiconductor that is exposed to sunlight and capable of absorbing it. In PEC cells, the two electrodes can be an n-type semiconductor photoanode and a working in-the-dark cathode, a p-type semiconductor photocathode and a p-type semiconductor photoanode, a p-type semiconductor photocathode and a working in-the-dark anode [11,12]. Our approach is based on using two semiconductors in a tandem configuration, where the semiconductor electrodes are excited by the same light beam, with the second electrode receiving the radiation diffused by the first one, as described in Fig. 1 and [13].

This configuration optimises sunlight adsorption (>75%) because the photovoltage is generated by the combination of the two electrodes' potential, allowing a sizeable solar spectrum coverage and a wide

* Corresponding author.
** Corresponding author.
E-mail addresses: orazio.barbera@itae.cnr.it (O. Barbera), giosue.giacoppo@itae.cnr.it (G. Giacoppo).

https://doi.org/10.1016/j.renene.2024.120154
Received 5 May 2023; Received in revised form 20 November 2023; Accepted 14 February 2024
Available online 15 February 2024

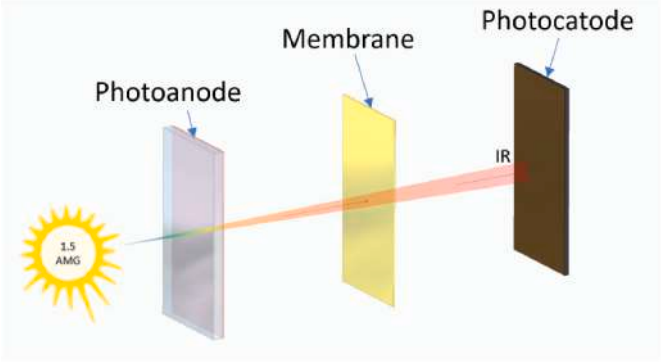

Fig. 1. A simplified schematic of a tandem configuration of a PEC cell with solid electrolyte and two active-semi conductive electrodes.

window of small bandgap materials to choose from, relaxing the stringent requirement of band-edge position to straddle the water redox potential and potentially achieving a higher efficiency than single semiconductor configuration. The research on PEC WS relies on semiconductor electrodes that exhibit appreciable photogenerated charge separation at the solid/liquid interface when illuminated by sunlight [14,15]. Several n-type semiconductors, including TiO_2, ZnO, $BiVO_4$, Ta_3N_5, WO_3 and Si, were studied as anodes for PEC WS. They show good potential but are characterized by a large bandgap and/or instability in the electrolyte solution. Among n-type semiconductors, hematite (α-Fe_2O_3) is characterized by the position of the low-valence band, abundance, stability in an aqueous electrolyte solution, non-toxicity, bandgap of about 1.9–2.2 eV, a solar radiation utilisation of almost to 40 % [16].

The WS performance of a hematite photoanode in a PEC cell, enhanced via Co-doping and surface modification, was studied in Ref. [17]. Altered electrode surface with catalysts to improve semiconductor efficiency using atomic deposition-growth of MnO_x on hematite was tested in Ref. [18]. Quick high-temperature annealing was used in Ref. [19] to enhance the performance of thin hematite layers on a TiO_2 nano-sheet. Hematite nanorod films, deposited on titanium foils and modified with phosphorous, were considered in Ref. [20]. A simple and fast method for nanostructured hematite production using an ultraviolet-assisted process was proposed in Ref. [21]. Performances and electronic properties of p-type CuO semiconductors were studied in Ref. [22], and the nanoscale structure of Cu/Cu_2O/CuO nano crystal's system was investigated in Ref. [23]. The preparation of Copper Oxide photocathodes was studied in Ref. [24], where a solution-based process was used for preparing the semiconductor, which was experimentally characterized in a PEC cell with a Pt counter electrode. A different method for Cu_2O/CuO photocathode preparation (fast annealing) was proposed in Ref. [25], whilst in Ref. [26], the semiconductor material was coated on an n-type Silicon electrode by varying the film deposition temperature. Other preparation techniques were studied in Refs. [27–30]. The main disadvantage of PEC cells is the difficulty in scaling systems characterized by large area, high modularity and efficiency, which can provide numerous advantages in power applications [31–34], enabling solar hydrogen production independently of any gas distribution infrastructure [35–37]. It is critical for implementing the hydrogen economy or complementing battery-powered power generation systems [38]. Further technical problems derive from managing the liquid and produced gases; in fact, additional energy is required in a post-processing phase to separate the produced hydrogen from the water, influencing the final performance of the prototype [39]. Corrosion problems also have a major impact on the practical development of the PEC cells and no relevant reports deal with the extensive operation of these devices. Most of the experiments reported in the literature for assessing the electrochemical performances are carried out in close-to-neutral sulphate and phosphate-buffered solutions, mitigating corrosion [40,41] but causing series-resistance issues in practical devices. Some attempts to obtain engineered devices mainly integrate a photovoltaic/thermoelectric system/PEM (Polymer Electrolyte Membrane) to the PEC cell or investigate one photoelectrode with Pt as a counter electrode. PEC cell prototypes with hematite photoanodes and liquid electrolytes were tested in Ref. [42], where authors investigated WO_3 and undoped hematite; in Ref. [43], where authors, using a half-cell, demonstrated that under microgravity conditions it is possible to produce hydrogen efficiently; in Ref. [44], where an integrated concentrated photovoltaic and photoelectrochemical hydrogen reactor was developed; and in Ref. [32] where a 50 cm^2 tandem PEC-PV cell named "CoolPEC" (compact, optimized, open light PEC cell) was developed. In Ref. [45], an engineered PEC cell was simulated with dome electrodes of 840 cm^2, a liquid-recirculated electrolyte and TiO_2 and Cu_2O-based electrodes. An 820 cm^2 active area PEC cell was developed in Ref. [44], in combination with a 36-cell solar panel. It produced hydrogen via photo electrolysis on the photocathode (a Cu_2O-coated stainless-steel semiconductor) and PEM electrolysis. In Ref. [46], a lab-scale PEC with an Ag/$NaNbO_3$ photoanode and a Pt counter electrode, immersed in a NaOH aqueous solution was developed, thermoelectric device was used as bias-voltage source. Several PEC-PV devices were presented in Refs. [11,47,48], where most prototypes are characterized by aqueous electrolytes and precious costly and non-hearth abundant materials. The above-described prototypes appear far from practical applications and can provide results of limited interest for large-area PEC cells. Our recent studies have been directed towards an innovative PEC cell, in tandem configuration, with a solid polymeric electrolyte membrane and non-critical raw materials (non-CRM) as semiconductors to overcome the technological problems described above, mostly found in cells with a single semiconductor and liquid electrolyte. This architectural choice allowed us to direct research towards heart-abundant and low-cost active materials, in particular hematite and copper oxide. The solid electrolyte, sandwiched between an n-type P- and Ti-doped Fe_2O_3 photoanode (PA) and a p-type CuO photocathode (PC), operates as a gas separator and electrolyte. Attention was focused on investigating non-CRM in a 0.25 cm^2 PEC cell, achieving a throughput efficiency of 2.9%. The anionic membrane was based on polysulfone polymer containing quaternary ammonium species [13,49–51]. Appropriate deposition technologies, including nano-columnar growth using cost-effective bath-deposition methods, spray deposition, and successive chemical/thermal treatments, were used as described in Refs. [13,50]. Using a hydrophobized gas diffusion layer (GDL) as a substrate for the CuO photocathode produced dry hydrogen and a relevant increase in throughput efficiency [49]. The above literature analysis reveals that a large-area PEC cell in tandem configuration capable of producing dry hydrogen using a solid electrolyte and a photocathode supported on a gas-porous and hydrophobic carbonaceous substrate is still not investigated. Consequently, the research activity proposed in this work aims to fill this gap in the scientific literature, studying the feasibility of an engineered PEC cell prototype that, starting from the concept developed in the 0.25 cm^2 cell (consisting of an extremely simplified cell architecture made for the development of active materials), leads to a device with a large active area and, above all, of practical interest. Numerous problems were addressed, including the isolation from leaks of liquids and gases through the use of suitable gaskets, the formation of an internal electrical connection, the management of water, hydrogen and oxygen, the correct clamping of the cell, the assembling of a three-layer membrane through glueing, in a design that is as simple and compact as possible and uses commercial-low cost materials. The paper offers the entire engineering process undertaken, the experimental test results and, in the appendix, numerous images and procedures demonstrating the considerable effort made, a video showing the hydrogen's bubbles formation was added as supplementary material. The achieved results demonstrate the goodness of the design adopted and indicate the way to adopt design improvements capable of increasing performance and obtaining cells of even

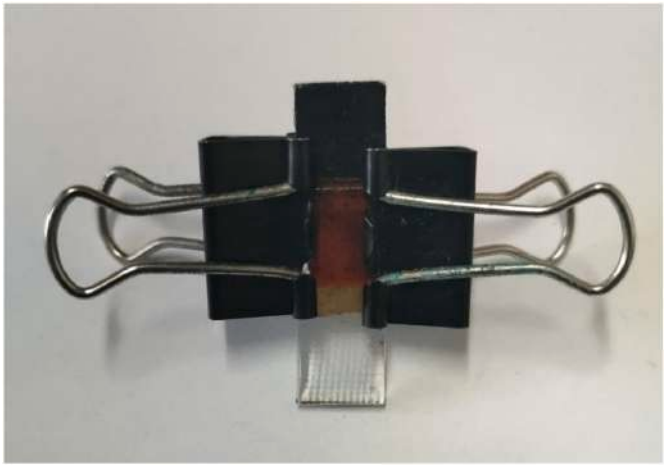

Fig. 2. Picture of the 0.25 cm^2 lab-scale cell with the hematite (orange), the GDL (black) and the two paper clips.

greater areas.

2. Experimental

2.1. Upscaled cell design

The 25 cm^2 PEC cell studied in this research work is the upscaled prototype of a lab-scale 0.25 cm^2 cell developed in Refs. [13,49–51] for evaluating the active materials. It is a PEC cell fed with water, with a tandem configuration based on a five-layer structure: an FTO glass supporting a layer of Fe_2O_3-based semiconductor as photoanode, a solid and sunlight transparent polymer alkaline membrane as the electrolyte, and a CuO-based photocathode supported on a carbonaceous gas diffusion layer (GDL, Sigracet 35BCE). As dehydrated hydrogen production represents one of the main goals of the research activity, the GDL was hydrophobized to allow the hydrogen to pass through the porous layer and block the distilled water between the GDL and the photocathode. The incident sunlight passes through the transparent FTO glass layer and reaches the Fe_2O_3 (hematite) photoanode, an n-type semiconductor absorbing the higher energy photons; the underlying CuO (Cupric Oxide) photocathode, a p-type semiconductor, absorbs the lower energy photons transmitted or diffused through the transparent polymer electrolyte membrane. According to our previous studies [13,49,51], a tandem cell works by generating electron-hole pairs at the anode and cathode, respectively, by interacting with incoming light.

In the Fe_2O_3-based photoanode, band edge bending drives photogenerated holes towards the electrolyte; the edge of its valence band is at a sufficiently high potential for triggering oxygen evolution from water. In the CuO-based photocathode, band bending drives photogenerated electrons towards the electrolyte; the edge of its conduction band is at a sufficiently low potential for hydrogen evolution from water. In the tandem cell architecture, all photons with energy above the narrower band gap, which should have a value close to 1 eV (1.25 eV for CuO), can contribute to the water-splitting process. The wide band gap oxide should possess a band gap of 1.65–2.1 eV (2.1 eV for Fe_2O_3). The band gaps of CuO and Fe_2O_3 are adequate for capturing most of the solar spectrum; approximately 75% of the incoming light energy can be utilized. From a physicochemical point of view, analysis carried out through SEM-TEM imaging techniques of hematite and CuO, the latter supported on a hydrophobized GDL, were previously reported by our group in Refs. [13,49,50] confirming the nanocolumnar structure of hematite and uniform hydrophobization of the GDL where CuO nanoparticles were deposited. The nanocolumn structure of hematite contributes to minimising the electron-hole recombination and facilitates the charge transfer between the photoelectrodes. The lab cell, used for the active materials characterization and the investigation of the WS performances of the hematite-cupric oxide couple, is characterized by a highly simplified design. As Fig. 2 shows, there are only three parts: the FTO glass supporting the hematite-based photoanode (red), the anionic membrane (not visible) and the GDL supporting the CuO-based cathode (black); two paper clips clamp the cell for the correct electrical contact.

In the 0.25 cm^2 lab-scale cell, there are no paths for water and produced gases, no tie-roads for clamping, and no specific path for current collection, directly drained from GDL and FTO by external contacts. Thus, it was necessary to rethink its concept completely to obtain a scaled-up device. In the first step, the active area of the scaled-up cell was set to 25 cm^2, representing a compromise between handling during experimental activities and studying the active area scaling effects. Since the active area of the scaled-up cell is 100 times larger than the lab-scale cell, it is reasonable to expect an influence of the scaled-up size on PEC cell performance. Fig. 3 shows an exploded view of the first concept of the scaled-up PEC cell, composed of 11 parts. Starting from the left side of Fig. 3, a "Support plate" made of a plastic material and equipped with 8 holes for the allocation of the screws and tightening of the hardware was designed; this component hosts two fittings for hydrogen collection

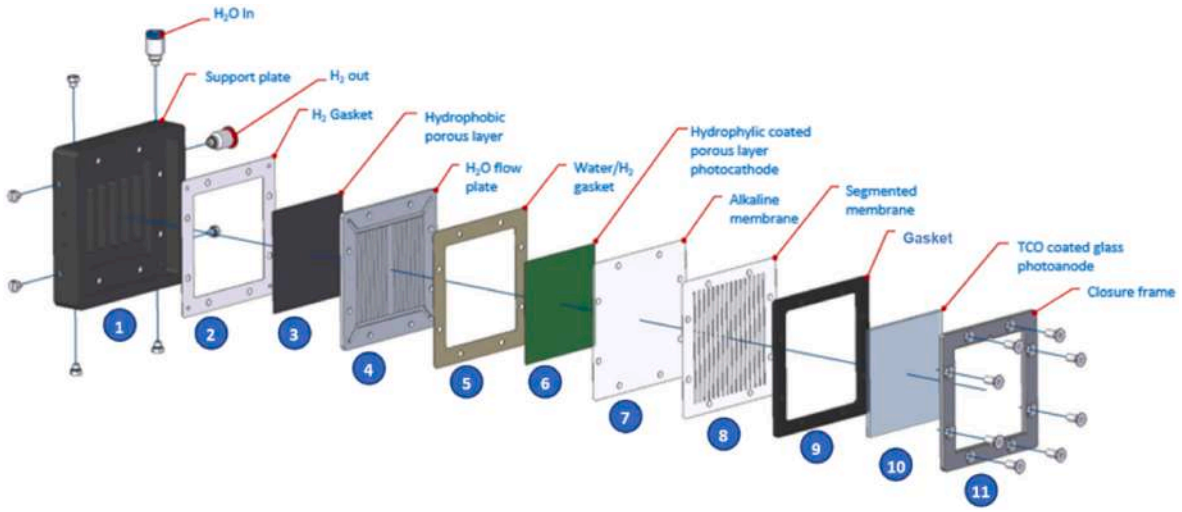

Fig. 3. First concept of the PEC cell, from left to right, the most important parts can be seen: (1) the support plate with the H_2O In and H_2 out fittings, (2) the H_2 Gasket, (3) the hydrophobic porous layer, (4) the H_2O flow plate, (5) the water/H_2 gasket, (6) the hydrophilic coated porous layer photocathode, (7) the alkaline membrane, (8) the segmented membrane, (9) the gasket, (10) the TCO-coated glass photoanode and the closure frame.

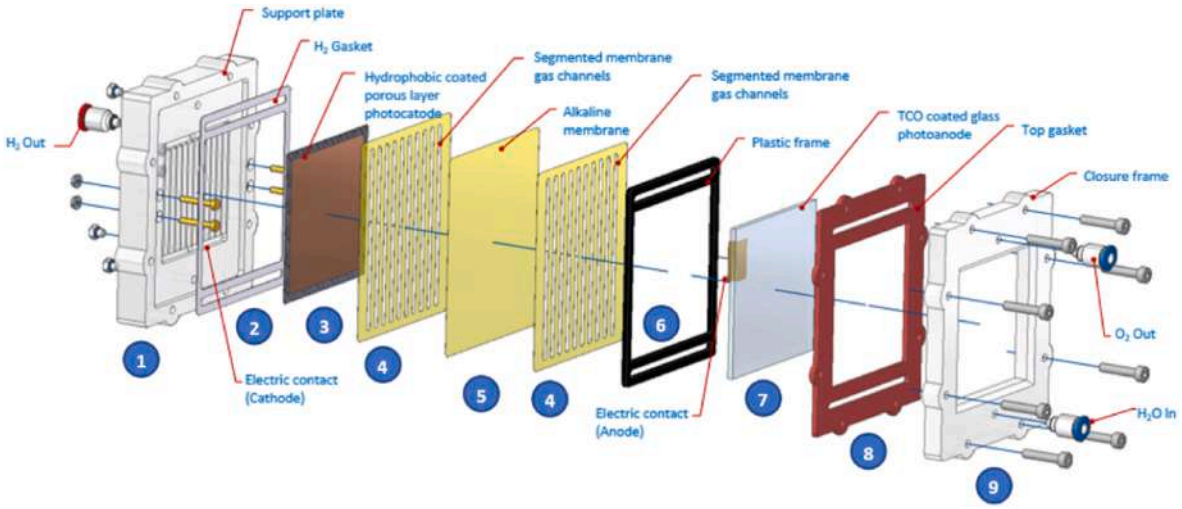

Fig. 4. The revised concept of PEC (second prototype), from the left to the right, the most important parts can be seen: (1) the support plate with the fitting for the H_2 (H_2 out) and the electric contacts (cathode), (2) the H_2 gasket, (3) the hydrophobic coated porous layer photocathode, (4) the segmented membrane gas channels, (5) the alkaline membrane, (6) the plastic frame, (7) the TCO-coated glass photoanode with the electric contact (anode), (8) the top gasket, (9) the closure frame with H_2O In and O_2 Out fittings.

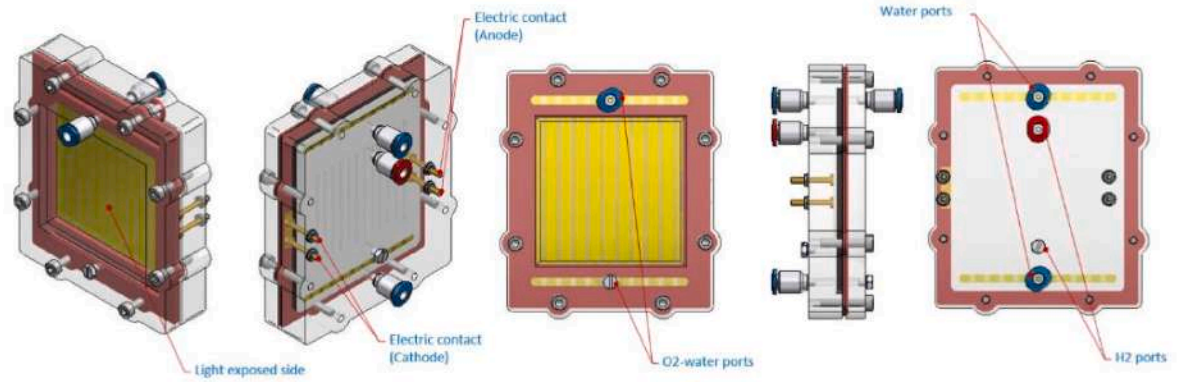

Fig. 5. Five different views of the assembled PEC: from the left, axonometric views of the frontal "Light exposed side" with fitting and rear dark site with electric contacts and fittings, frontal side with O_2 water ports, and rear views with water ports and H_2 ports.

("H_2 out") and water inlet ("H_2O in"), other plugs were foreseen for connecting several units in series or parallel. A PTFE gasket ("H_2 gasket") is seated on the support plate and prevents hydrogen leakage; the central window of the gasket allocates the "hydrophobic porous layer" placed in contact with the rear part of the "H_2O flow plate". This component was conceived as a graphite-based part that hosts the distilled water flow field. The open channel lands allow the water to reach the photocathode and the produced hydrogen to pass through the hydrophobic porous layer before exiting the cell. The "Water/H_2 gasket" is placed upon the graphite plate with the "Hydrophilic coated porous layer photocathode". The "Alkaline membrane", coupled with the "Segmented membrane", are the parts that form the solid electrolyte; a third "Gasket" is placed onto the solid electrolyte and seals the "TCO-coated glass photoanode" from leakage. Finally, the metallic "Closure frame" clamps the whole assembly. All parts are stacked, as illustrated in Fig. 3 and compressed by the closure frame with the screws.

Distilled water is fed through the support plate to the H_2O flow plate made of graphite, which has two functions: distributing water over the packed assembly (photocathode/membrane/photoanode) and collecting current and hydrogen. The channels machined on the surface of the "H_2O flow plate" are perforated, allowing the produced hydrogen to pass through the hydrophobic layer to the collection chamber in the support plate. The hydrophobic layer behind the H_2O flow plate blocks the liquid water between the flow plate and photocathode, allowing the gaseous hydrogen to pass through and exit the cell in a dehydrated form. Concerning the anodic side, produced O_2 is collected at the top of a two-layer membrane (segmented membrane) channels and vented out the PEC cell through a specific hole in the closure frame. Gaskets are used for leakage prevention. The difference with the lab-scale cell is significant; the design was driven by the requirement of O_2 and H_2 separation, a dry H_2 collection, no gas leakage, a safety vent of the O_2 to the external, current collection through a dedicated path, the robustness of the case for a correct clamping and a resistance to the high temperature generated by the solar simulator lamp. These aspects were not considered in the lab-scale cell because of the minimal amount of gases that were free to vent out due to the absence of gaskets, the indirect measurement of the produced H_2 only by current monitoring, and the small and enough water content trapped in the membrane.

2.2. Design, optimization of the prototype, manufacturing and assembly

The first concept of the PEC cell was revised and re-designed to reduce the number of parts and contact interfaces, as illustrated in Fig. 4.

Starting from the left side of Fig. 4, a plastic "Support plate" hosts the "H_2 gasket" made of expanded PTFE and supports the "Hydrophobic coated porous layer photocathode" placed in the central window of the

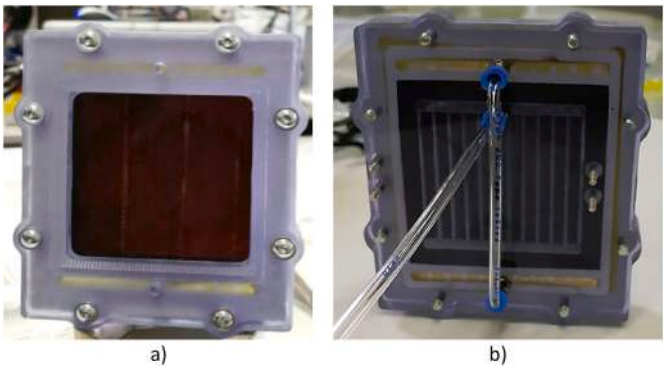

Fig. 6. PEC cell assembled with pipe connection ready for characterization tests; a) front view (light-exposed side), b) rear view (side working in the dark).

gasket. The electrolyte is formed by three layers of polymeric membrane (the "Alkaline membrane" placed in between two "Segmented membrane gas channels") and is stacked on the surface formed by an "H_2 gasket" with the photocathode inserted. A second (black) "plastic frame" maintains the "TCO coated glass photoanode" in contact with the "segmented membrane gas channel". To keep in place the "TCO coated glass photoanode", a "Top gasket" with a smaller central window was adopted in such a way as to cover the interface between the glass and the underlying gasket and allow the plastic "Closure frame" to transfer the clamping force to the cell assembly. The electrical connection is made of a thin copper foil ("Electric contact (Anode)"), which is in contact with the "TCO coated glass photoanode" and with conductive pins ("Electric contact (cathode)") inserted in the "Support plate". In this new configuration, the water inlet ("H_2O In") and the oxygen outlet ("O_2 Out") are placed on the opposite side of the hydrogen outlet ("H_2 Out"), the graphite-based "H_2O flow plate" was eliminated and distilled water fed from the cathodic side.

Moreover, the three-layer membrane (instead of two) consists, as Fig. 4 depicts, of a solid membrane ("Alkaline membrane" in Fig. 4) sandwiched between two "Segmented membranes" where a series of parallel channels are made on the surface using a laser cutting machine. These segmented membranes drive the produced gases from the photoactive regions to the outlet ports and collect the liquid water in intimate contact with the photoelectrodes and the anion-exchange "Alkaline membrane". In principle, assembling three membranes instead of engraving the channels on one monolithic membrane made manufacturing much more effortless. Moreover, a "specific" highly hydrophobic layer was introduced on the photocathode side to create a barrier for the liquid water only and produce hydrogen as dry as possible. Two plastic frames and sealings lay all the components in place, avoiding water and gas leaks. The graphite flow plate, which was foreseen as H_2O/H_2 distributor/collector, was substituted by a segmented membrane (as on the anodic side), and the hydrophobic and hydrophilic porous layers were integrated into one piece. Therefore, the number of active parts was reduced, and a simplified cathode flow path was obtained. In principle, the water supply method is simple as it is static. The cell has to be filled with distilled water through the appropriate fittings ("H_2O In" in Fig. 4, "Water ports" in Fig. 5) and is consumed by the photoelectrochemical reaction. Therefore, it is unnecessary to have a way out of the liquid but a periodic filling (which can be done manually or by gravity). Concerning the final assembly, a preliminary check was carried out by digital prototyping, allowing the virtual validation of the PEC cell design regarding the fluids path, mechanical interferences, and alignments. Fig. 5 shows different views of the virtual assembly of the 25 cm^2 active area PEC cell.

Once the design of the PEC cell was validated and the materials for each part were chosen, the last step involved manufacturing the parts. Plastic materials of unit cell hardware, namely the "support plate" and the "closure frame", were processed by a milling machine. This manufacturing method is suitable in case of a limited number of samples; other processes, such as thermal forming or injection moulding, are mainly used for large-volume production due to the high initial cost of the moulds (in the order of tens of thousands of euros). Laser cutting technology is the best option for the "soft components" like gaskets and membranes for the possibility of rapidly changing the design with a low cost of machine set-up. Also, in this case, other technologies (i.e. the die–punch) are costly due to the tooling cost and machine set-up. Generally, materials used for PEC cells should withstand sun irradiation and weathering agents and be compatible with the alkaline environment within the cell. The case material and closure are made of polyvinylidene fluoride (PVDF), which is compliant with the external agents and the alkaline environment and shows good mechanical properties, allowing the PVDF "support plate" and "closure frame" to be effective in resisting the compression load exerted by the eight bolts. Gaskets are made of Expanded Teflon or silicone characterized by a Shore A hardness range of 35–40, allowing for a suitable cell sealing without excessive stress on the FTO glass, even with a low clamping torque of the bolts. FTO glass represents the most fragile part of the PEC assembly, and misalignments of stacked parts, concentrated loads, or lack of planarity can easily compromise its integrity. After manufacturing and supplying the parts, the unit cell was assembled. A detailed description of the assembly procedure can be found in Figure A.1 of Appendix A.

The final assembly of the unit cell is shown in Fig. 6; the front view, which is exposed to sunlight, is shown in Fig. 6a, whilst the rear of the cell, the dark side, is shown in Fig. 6b with plastic tubes connected for hydrogen collecting and water feeding.

2.3. *Membrane and FTO glass scaling–up, issues and solutions*

A Fumasep® FAA3-50 membrane from "FUMATECH BWT GmbH" (Bietigheim-Bissingen, Germany), with a nominal thickness of 50 μm, was used as the anionic electrolyte. It is based on a brominated polysulfone backbone with quaternary ammonium side chain groups and supplied in bromide form (Br^-). It was treated in 1 M NaCl solution for 72 h to obtain its chloride form (Cl^-) and to purify from production residuals, and, before electrochemical tests of tandem PECs, it was conditioned in a fresh 1 M KOH solution for 24 h to make an OH^- form [51]. To scale up the three-layer electrolyte, the membranes in bromide form were separately cut with a laser machine in the desired shape (Figure A.2a of Appendix A), forming the channels as planned in the second revision of the prototype. A first adhesion test was performed on a geometrical configuration to obtain a single-layer membrane. A hydroalcoholic ionomer dispersion (water-ethanol) was deposited on the first layer (where the flow field is cut), placed onto the solid intermediate-layer membrane, and dried in a press at 40 °C for 10 min applying a pressure of 50 kg/cm^2. In the second step, the third layer, with the flow field, was painted with the hydroalcoholic ionomer dispersion, placed on the other side of the solid intermediate-layer membrane, and dried in the press with the same operative conditions (Figure A.2b of Appendix A). A perfect adhesion was obtained on both sides. The three-layer membrane was then converted into the hydroxide form (Figure A.2c of Appendix A), and no detaching was observed. The second adhesion test was performed after the NaCl treatment (Cl^- form) in a scaled-up membrane (Figure A.3 of Appendix A).

The most critical issue was the swelling process that occurs with the hydration of the polymer membrane. The initial dimensions of the three-layer membrane in water (OH^- form) were 6.2 × 7.4 cm; if left in water for 24 h, it reached the maximum dimensions of 7.5 × 9.0 cm with an isotropic increase of about 20%. The swelling of the membrane caused an enormous dimensional variation and, in the segmented one, the loss of the channel shape. Consequently, handling and assembling it in the correct position was complicated. Since the production of paths onto polymeric membranes is CO_2-Laser assisted [52], a new, most effective approach was found to overcome the limitations of the segmented

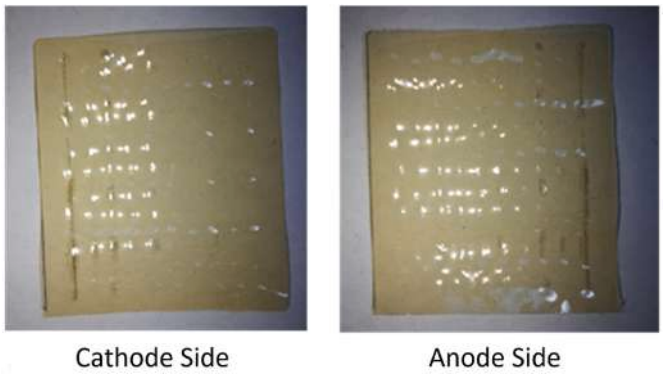

Fig. 7. Cathode and Anode sides of the ablated FAA3-50 membrane.

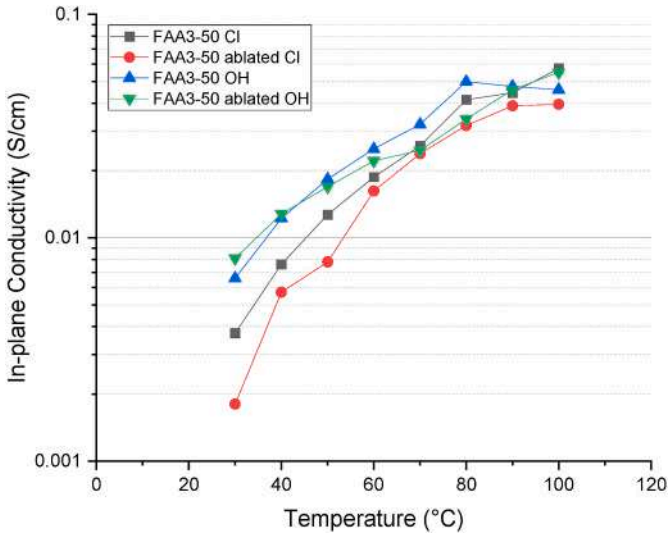

Fig. 8. Anion conductivity comparison between ablated and "as it is" membranes in Cl- and OH- form.

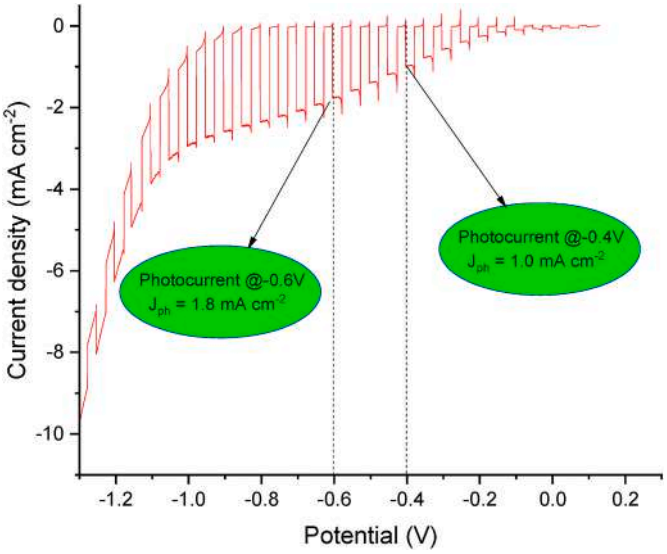

Fig. 9. On-off illumination experiments of the optimized FTO/Fe_2O_3+Ti/FAA3-ION//FAA3-50//FAA3-ION/CuO PEC in 0.25 cm^2 lab scale.

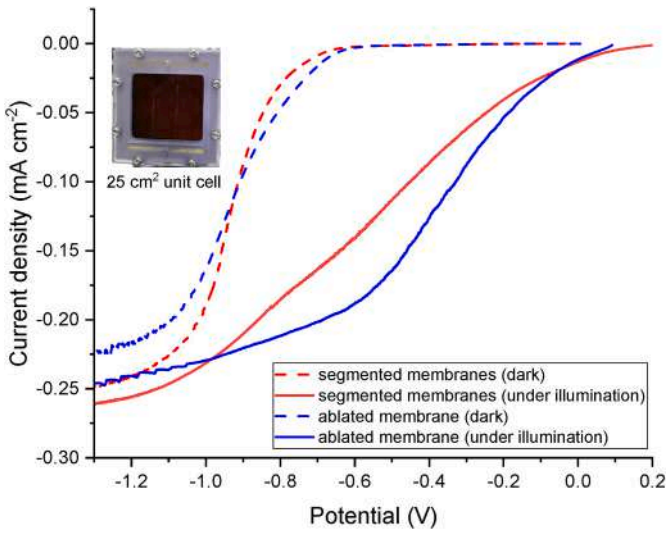

Fig. 10. Current density in 25 cm^2 PEC cell in dark conditions and under illumination with segmented membranes (red lines) and ablated membranes (blue lines).

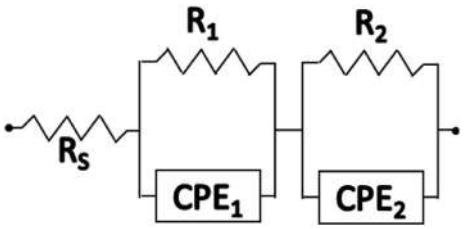

Fig. 11. Equivalent electrical circuit, under illumination, of a photoelectrochemical cell.

membranes. In particular, laser ablation was performed on the surface of the membrane to make surface corrugation instead of flow fields. The surface was corrugated, placing the membrane on the vacuum table of the laser machine. Different tests were carried out to verify if the ablation process can modify the properties of the membrane. The membranes with Cl^- counterions were subjected to the ablation process and then physicochemical characterized in terms of ion exchange capacity (IEC), UV–Vis spectra, and anionic conductivity and compared to the pristine membrane. The ablated membrane is shown in Fig. 7.

The glass, subject to thermal stress during the hematite deposition process, presented significant problems of flatness and embrittlement. Figure A.4 of Appendix A shows how the glass lost the initial flat shape after hematite preparation. The loss in flatness, combined with embrittlement due to the photoelectrode thermal treatment, led to the breaking the FTO glass during the unit cell assembly. Figure A.5 of Appendix A shows the unit cell with the broken FTO glass; this has precluded using this initial prototype for the experimental activity. Such issues were overcome by lowering the annealing temperature to form hematite nanocolumns (from 750 °C to 650 °C), and the shape of the FTO glass remained unchanged. Specifically, several ceramic tiles were tested as supports for the FTO during thermal treatment, choosing the one that ensured the planarity and smoothness of the glass plate. UV–visible–NIR measurements were carried out with Cary Win UV 6000 (Agilent Technologies) in the 2000-200 nm spectral range. The absorbance of the Fumasep® membrane or ablated membrane based on Chloride (FAA3-50 Cl^-) and hydroxide (FAA3-50 OH^-) was investigated after zeroing the dual beam instrument. The detailed procedure for measuring the ion exchange capacity (IEC) and anion conductivity is reported elsewhere [53].

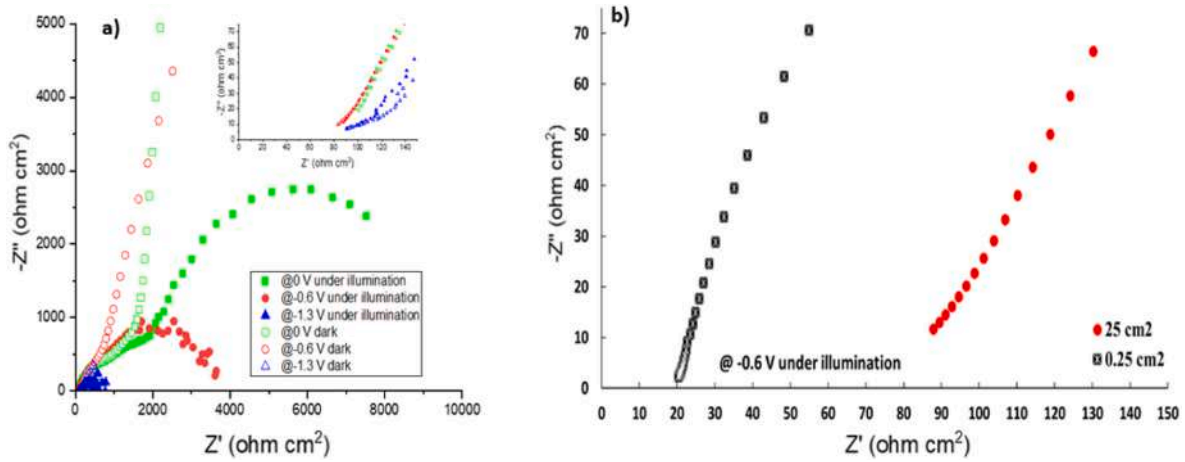

Fig. 12. a) EIS, at high frequencies, spectra comparison under illumination of 0.25 cm^2 vs 25 cm^2, b) EIS spectra at different conditions (light and dark) and applied voltages for the upscaled cell (magnification of EIS spectra in the high-frequency range in the inset.

2.4. Electrochemical characterization of PEC cell prototype

The measurements were carried out using the upscaled PEC cell; for the first investigated test, the cell was equipped with titanium-doped hematite deposited over FTO glass as the photoanode; ablated and segmented-three-layer anionic membrane electrolyte, and the GDL substrate coated with copper oxide as the photocathode. An ionomer dispersion was deposited over the electrodes. Such a dispersion consisted of 5 wt% of anionic ionomer having the same composition as the FAA-3 membrane and was obtained using a mixture of n-propanol and ethanol (1:1 wt). A concentration of ionomer corresponding to 25 μL cm^{-2} was deposited for both the photoanode and photocathode. Then, the electrodes were conditioned in 1 M KOH for 1 h before the assembly discussed in the previous sections.

Electrochemical impedance spectroscopy (EIS) was carried out in the range of frequency 100 kHz-1 Hz and 50 mV of amplitude at 0 V and two bias-assisted potentials (−0.6 and −1.3 V).

The H_2, H_2O, and CO ionic currents were quantified using a mass spectrometer ThermoStar™ GSD320.

3. Results and discussion

3.1. Membrane characterization

UV–Vis spectroscopic measurements were performed on the sample in Cl^- form and after the ion exchange in OH^- form, as reported in Figure A.6 of Appendix A, to verify the effect of the laser ablation on the optical properties.

The ablation does not produce any optical modification of the polymeric membrane. The membrane remains transparent to the visible light after the ablation process and after the ion exchange in KOH for 24 h, meaning the full applicability of this procedure.

The ion exchange capacity (IEC) demonstrated that no modification of the surface groups is evident. An IEC of 1.85 meq/g was measured for the ablated FAA3-50 membrane with chloride as a counter ion, corresponding to the nominal one. For further confirmation, anion conductivity tests were performed on the samples in Cl^- and OH^- form before and after the ablation process. The comparison is shown in Fig. 8.

The measurement was carried out as reported elsewhere [53] in the temperature range from ambient up to 100 °C. This range was selected to stress the polymer at high temperatures and to simulate a local hot-spot in case of assembling in a large area cell or panel under the sun illumination. The conductivity of the membrane in OH^- form is higher than in Cl^- form due to the higher mobility of hydroxide ions. After the ablation, a slight conductivity reduction for FAA3-50 Cl ablated sample up to 60 °C was recorded, probably due to a dehydration effect during ablation. Over this temperature, the conductivity is comparable. The trend is the opposite regarding the samples with hydroxides as counterions; the conductivity is quite similar from 30 °C up to 60 °C, and a slight reduction is detected above this temperature. Also, this test confirms the practical applicability of the ablation process, meaning that this membrane can sustain a significant rise in the temperature inside the module while maintaining good conductivity and mechanical stability.

3.2. Single-cell test

The reference PEC cell, as reported in the previous papers [13, 49–51] regarding the optimization of a 0.25 cm^2 active area, was formed by Ti-doped hematite supported on FTO at the photoanode, anionic Fumasep® membrane acting as both gas separator and electrolyte and hydrophobized Sigracet substrate in which CuO was deposited as a photocathode. An ionomer loading of 25 μlcm^{-2} was added before cell assembly on PA or PC. In the on-off illumination experiments, shown in Fig. 9, 1.7 % enthalpy efficiency and 3 % throughput efficiency were obtained at −0.6 V.

Fig. 10 shows the electrochemical results for the upscaled 25 cm^2 prototype in dark conditions (dashed lines) and under illumination (continuous lines). The red I–V curves in Fig. 10 are related to the PEC cell equipped with the segmented three-layer membrane. The current density value in the dark is close to 0 mA cm^{-2} up to 0.6 V, demonstrating that no undesired secondary reactions are revealed in the region of interest. The photocurrent density, i.e. the difference between current density under illumination and current density in the dark, is about 0.14 mA cm^{-2} at 0.6 V in the bias-assisted region; consequently, the efficiency is, in this case, about 13 times lower than that achieved with the 0.25 cm^2 lab-cell.

The I–V curves in the blue colour (Fig. 10) are related to the cell equipped with an ablated FAA-3 membrane as the electrolyte. An increase in the photocurrent density and enthalpy efficiency (38% about) is revealed, passing from 0.13% with segmented membrane to 0.18 % with the ablated membrane-based prototype, whereas the performance is still ten times lower than the 0.25 cm^2 lab-cell.

A first qualitative analysis of Nyquist spectra allows us to distinguish between series, ohmic and polarisation resistance. The high-frequency intercept of the semicircles on the x-axis of the Nyquist plots is associated with the ohmic resistance (more precisely reported as series resistance, Rs). The difference between the low-frequency intercept in the Nyquist plot and Rs is assumed as the polarisation resistance (Rp). The total resistance corresponding to the low-frequency intercept on the

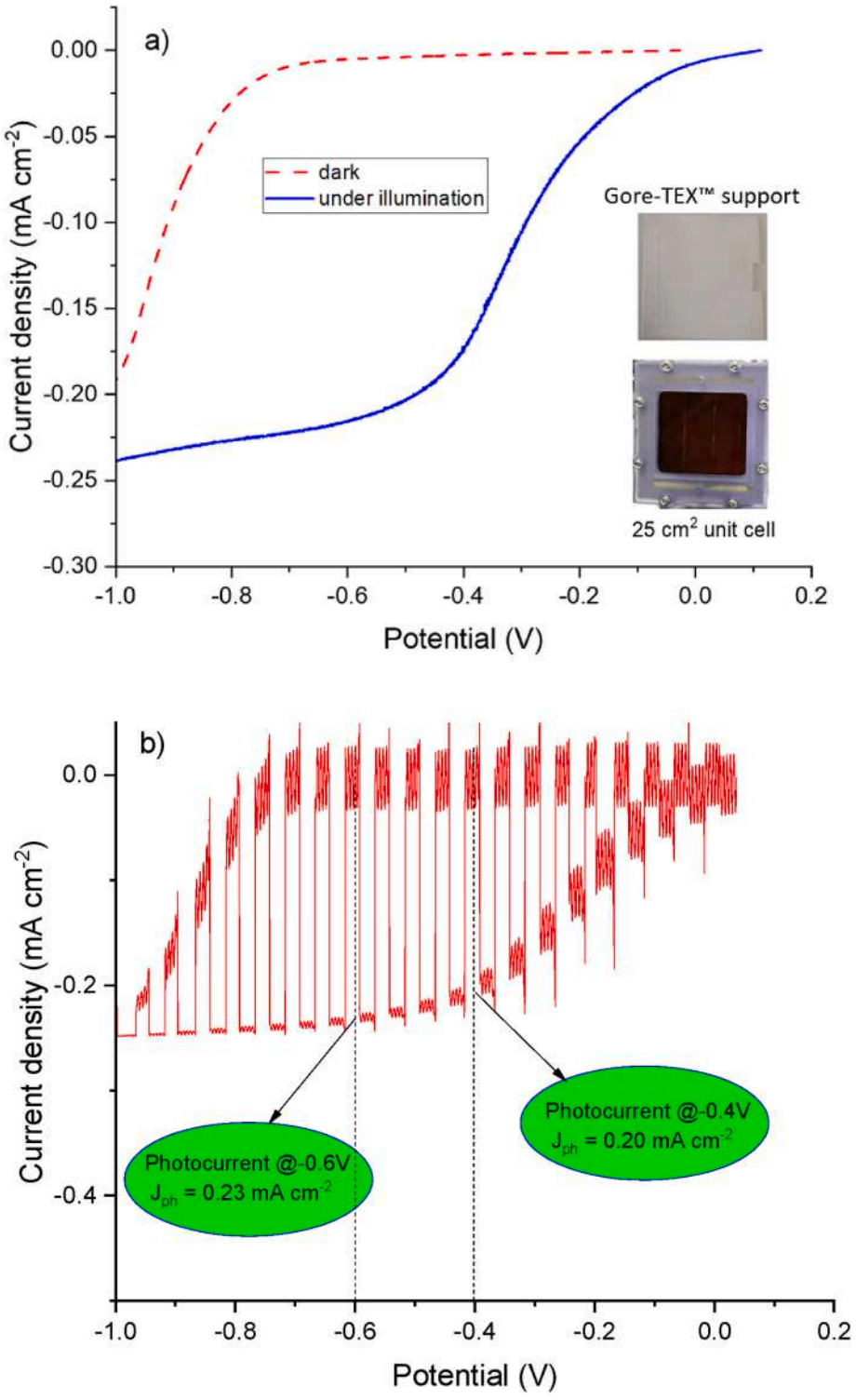

Fig. 13. Current density a) under illumination and in the dark and b) in the on-off illumination experiment for the 25 cm^2 prototype with Gore-TEX support under GDL.

abscissa in the Nyquist plot (Rs + Rp) corresponds to the differential resistance of the polarisation curves.

The equivalent electrical circuit (Fig. 11), under illumination, includes an ohmic resistance (series resistance) connected in series with two components, each consisting of a parallel between a resistance and a constant phase element (CPE). The series resistance reflects the ohmic phenomena, whereas the R//CPE components are associated with the electrode-electrolyte interfacial properties and related faradaic processes.

The Nyquist spectra of the cell under dark conditions are very similar at the different values of the imposed cell potential (Fig. 12a). The trend is, in fact, purely diffusive, following the fact that under dark conditions, even at three different cell potentials (0, -0-6, −1.3 V), the water-splitting reaction does not take place. On the other hand, under light conditions, an evident decrease in polarisation resistance can be seen as the cell potential increases. Under short-circuit conditions (0 V), the

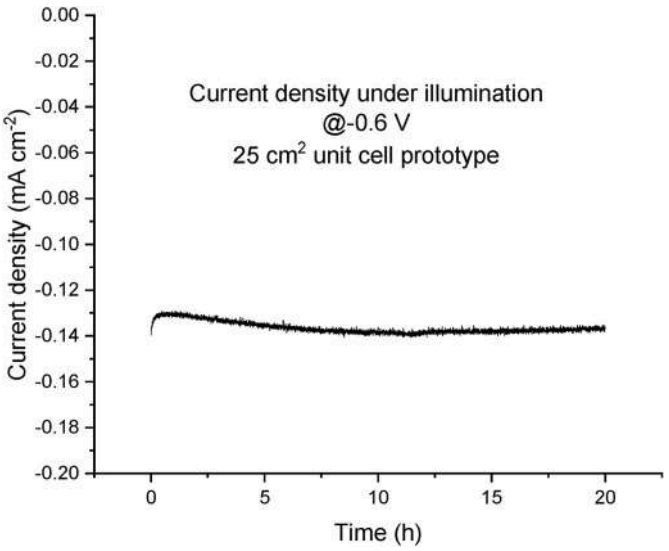

Fig. 14. Potentiostatic stability test, under illumination, at −0.6 V.

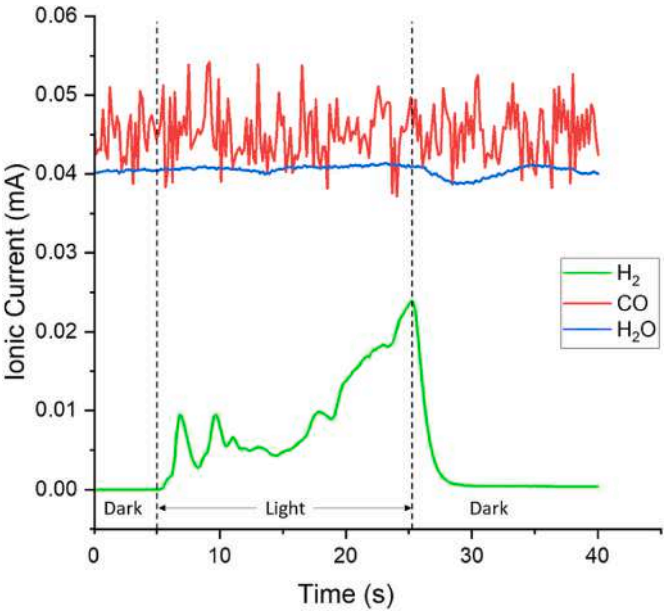

Fig. 15. The ionic current of H_2, H_2O and CO during chronoamperometry @ −1.1 V.

reaction (evident by the presence of the two photoanodic and photocathodic reaction semicircles) of water splitting is already present. However, the polarisation resistance values are very high; consequently, the photocurrent (as shown in the polarisation graphs) is very small. Furthermore, it is evident that the polarisation resistance values as the cell potential increases decrease from about 4000 Ω cm^{-2} at −0.6 V to about 600 Ω cm^{-2} at −1.3 V. This decrease leads to a substantial increase in the photocurrent value.

The analysis of the electrochemical impedance spectra comparison (Fig. 12b) shows that the polarisation resistance is the rate-determining step.

It can be deduced that the low photocurrent is due to a higher electrode/electrolyte interfacial resistance than in the lab cell.

In these terms, the discriminant of the performance gap between small (0.25 cm^2) and large (25 cm^2) area cells is the increase of series resistance, which is four times higher than in the lab cell (80–90 Ω cm^2 vs 20 Ω cm^2, Fig. 12b). It is due to the poor quality of the interfacial contact, which is related to the low compression force between the components. The contact pressure between the membrane and photoactive components was studied with a pressure-sensitive film to understand this issue better. The pressure-sensitive film replaced the membrane in 0.25 and 25 cm^2 cells to visualize the contact pressure as a red-scale colour map. As Figure A.7 of Appendix A shows, the contact pressure of the scaled-up PEC cell is significantly lower than in the lab cell. The following reasons can explain this: 1) low clamping pressure applied, 2) poor manufacturing tolerances and 3) insufficient stiffness of the closure frame.

Many strategies can be adopted to increase the contact pressure between photo electrodes and the membrane; in this case, a soft material was inserted under the GDL. This approach led to a considerable improvement (approximately 50%) in the photocurrent from 0.12 to 0.21 mA cm^{-2}, as shown by comparing the photocurrent at 0.4 V in Figs. 10 and 13. It confirms the fundamental role of the contact pressure in the photocurrent generation and the need to improve the clamping system of the scaled-up cell.

In terms of performance stability under illumination, a potentiostatic test at −0.6 V was carried out (Fig. 14), highlighting an extraordinary constant operation for 20 h with negligible photocurrent decay.

To verify that the measured photocurrent is related only to the hydrogen production, the ionic currents of H_2, H_2O, and CO were qualitatively measured by a spectrophotometer during a potentionstatic test at −1.1 V, where the cell was operated switching from dark to light. Fig. 15 shows that the ionic current signal of H_2 starts increasing at light on and rapidly decreases at light off (dark region). Conversely, H_2O and CO ionic currents did not show appreciable variation along the test.

These remarkable results for the selective hydrogen formation from PEC WS were related to using a polymeric membrane for H_2/O_2 separation and a hydrophobic backing layer for H_2O/H_2 filtration. In our case, the predicted value of STH efficiency for the Fe_2O_3/CuO tandem couple was 11%, combining 2.2 eV and 1.0 eV band gap oxides [54]. Thus, the obtained experimental value should increase by hindering recombination losses (appropriate use of co-catalysts) and optimizing interfacial components and bubble flow. However, this tandem cell architecture, working at a low bias (0.4–0.6 V), enables excellent utilisation of the incoming solar spectrum, and it may be considered an additional tread in photoelectrochemistry research. The feasibility of PEC scalability for achieving pure and green hydrogen production was demonstrated by employing cheap and non-critical raw materials. The biggest challenge of this technology for large-scale commercialization is achieving a bias-free PEC cell WS by employing inexpensive and earth-abundant materials in combination with the facile scalability of the components. The achievement of larger photocurrent and consequently relevant solar to hydrogen efficiency could be obtained in the future by enhancing the light intensity adsorption of the tandem cell through optimization of both the electrode thickness and the use of efficient non-CRM co-catalysts such as nickel alloys as well as the substitution of the polymeric membrane with a more performing solid electrolyte.

Regarding a scalable prototype representing the core of this manuscript, future work should be focused on either effective glass electrode membrane assembly (GEMA) to improve the interface between membrane and photoelectrodes or drilled FTO to facilitate the escape of oxygen flow through the photoanode outlet.

4. Conclusion

A large area (25 cm^2) PEC cell was developed in tandem configuration and using an anionic Fumasep® membrane as a solid polymeric electrolyte. The cell consisted of cheap semiconductors based on hematite and CuO deposited on FTO and hydrophobized GDL, respectively, specific gaskets, current collectors, closure frame, and flow fields for oxygen/water transport at the photoanode and H_2 transport at the photocathode.

Significant efforts were made to have, for the first time, an engineered and operational PEC cell with an active area 100 times higher than the lab scale one. The prototype is characterized by an appropriate design that efficiently manages reactants and products, the current collection, and the sealing of the whole system. At relatively low bias-voltage (0.4–0.6 V), the recorded photocurrent and efficiencies were higher than 0.2 $mAcm^{-2}$ and 0.2%, respectively. Further improvements to the present configuration are also highlighted and concerns mainly the increase of the interfacial contact between the membrane and the photoactive electrodes.

Interface issues between electrodes and solid electrolytes were also confirmed by EIS measurement, where high polarisation resistance was recorded compared to the 0.25 cm^2 reference lab cell.

On the other hand, durability experiments demonstrated good resistance to corrosion, showing a constant photocurrent after 20 h testing at 0.6 V in the bias-assisted region.

Moreover, hydrogen release from photoelectrochemical water splitting at the cathode side was confirmed by a mass spectrometer measurement, evidencing a selective production of pure hydrogen at the cathode side of the PEC WS cell.

CRediT authorship contribution statement

O. Barbera: Conceptualization, Methodology, Writing – original draft, Writing – review & editing. **C. Lo Vecchio:** Data curation, Investigation, Writing – review & editing. **S. Trocino:** Data curation, Investigation, Writing – review & editing. **A. Carbone:** Investigation, Visualization. **A.S. Aricò:** Funding acquisition, Project administration, Supervision. **V. Baglio:** Writing – review & editing. **G. Giacoppo:** Conceptualization, Methodology, Writing – review & editing, Visualization.

Declaration of competing interest

The authors declare that they have no known competing financial interests or personal relationships that could have appeared to influence the work reported in this paper.

Acknowledgement

Authors gratefully acknowledge funding from the European Union's Horizon 2020 research and innovation program under grant agreement no. 760930 (FotoH2 project).

Appendix A. Supplementary data

Supplementary data to this article can be found online at https://doi.org/10.1016/j.renene.2024.120154.

Appendix A

A.1 Unit cell assembly procedure

The unit cell assembly started from the "Support plate" where the current collectors were inserted (Figure A1a). Then, the H_2 gasket, the porous "Hydrophobic coated porous layer photocathode" (Figure A1b), and the three-layer segmented membrane (Figure A1c) were stacked in this order. The FTO glass supporting the photoanode and the relative "plastic frame" (gasket) were settled with the hematite electrode facing the membrane (Figure A1d). Finally, the "Top gasket" for preventing water/O_2 leakage was applied (Figure A1e) and compressed on the other stacked components through the "Closure frame" (Figure A1f), using a torque wrench of about 1 Nm per tie-rods.

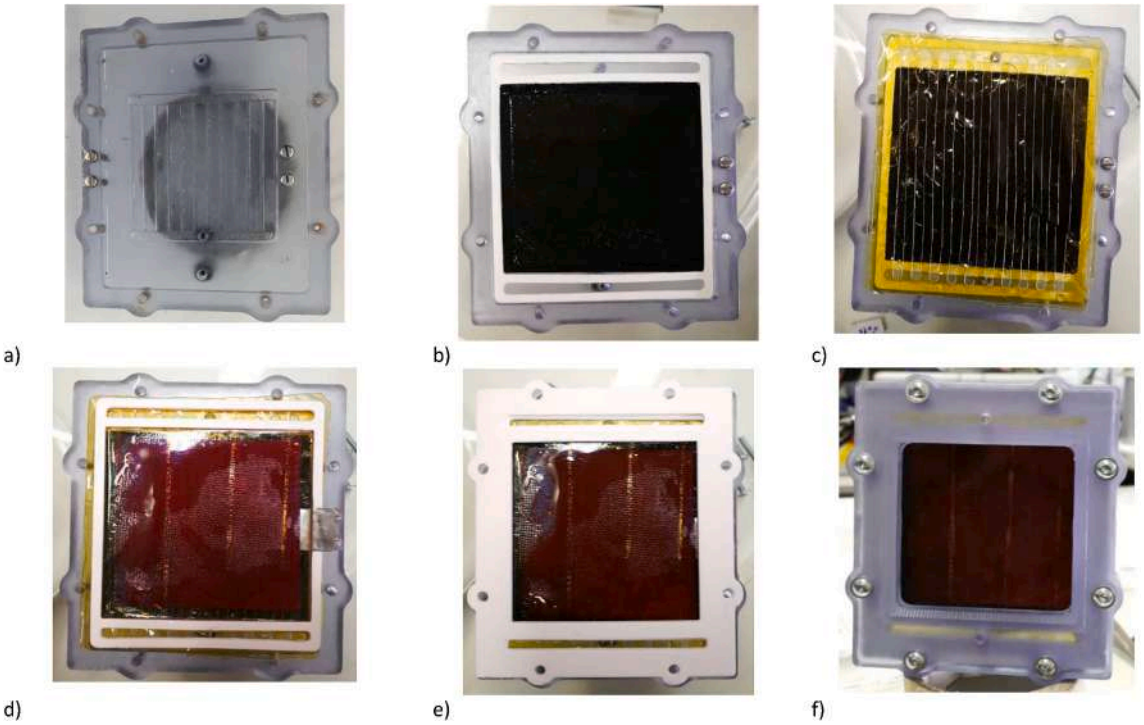

Fig. A1. Assembly of PEC cell: from left, a) Support plate, b) the Hydrophobic coated porous layer photocathode with the gasket in place, c) the three-layer segmented membranes in place, d) Plastic frame (gasket), FTO glass and collector slab (Electric contact Anode), e) Top gasket, f) Completed PEC assembly.

A.2 The 3-layer membrane

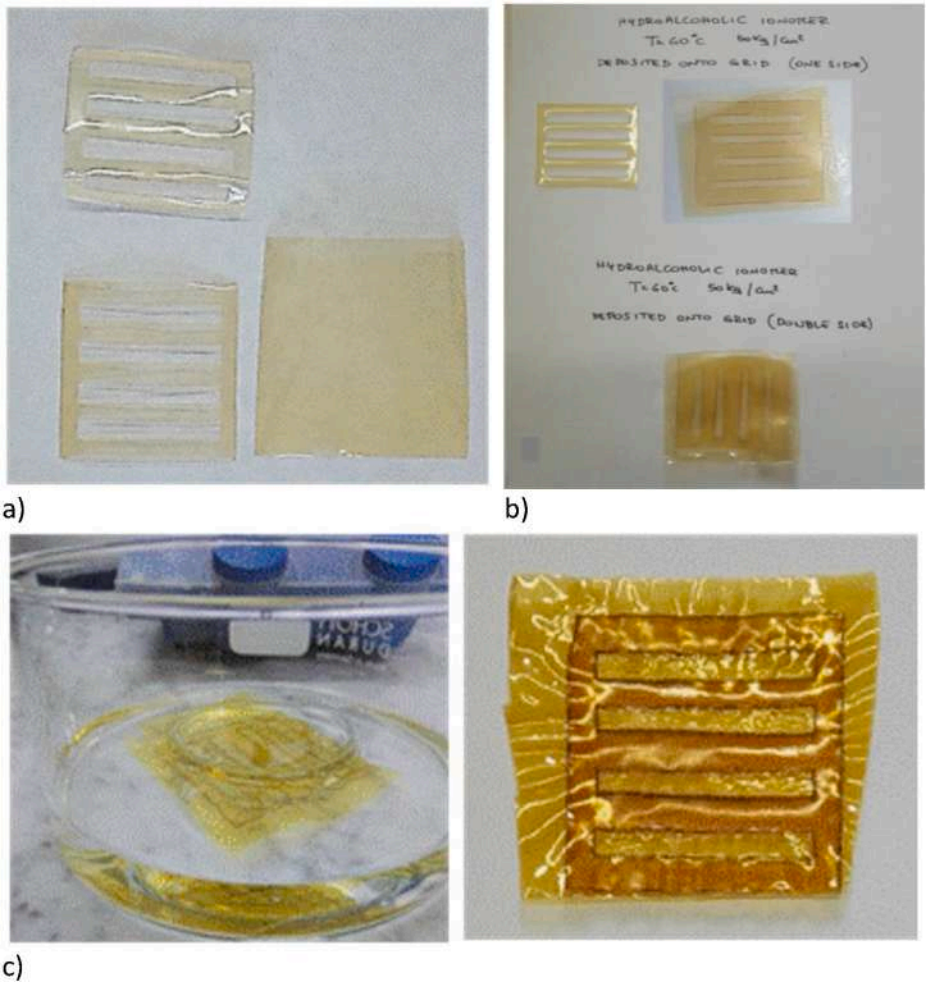

Fig. A.2. 3-layer membrane realization.

Fig. A.3. 3-layer segmented membrane. (a) The laser-cut flow field, (b) an adhesion test using the hydroalcoholic ionomer. As can be seen from two points of view, the adhesion obtained was not optimal, and the drying process led to the detaching of layers, (c) using an alcoholic ionomer as adhesive, partial solubilization of the membrane occurred.

A.3 Glass breakage and deformation issues

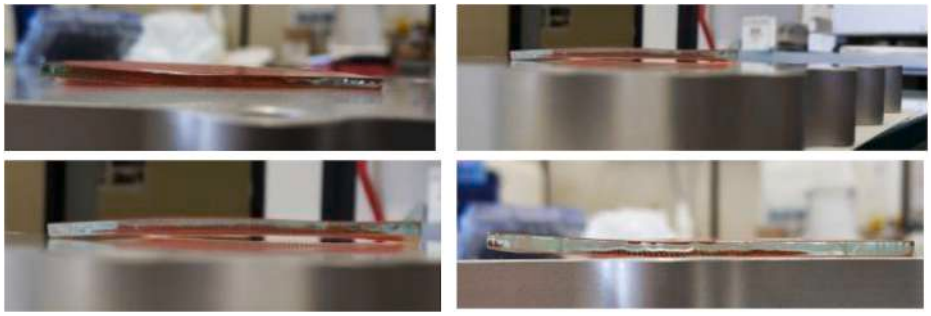

Fig. A.4. FTO glass deformation after the hematite deposition process.

Fig. A.5. Unit cell with broken FTO glass.

A.4 Effect of laser ablation

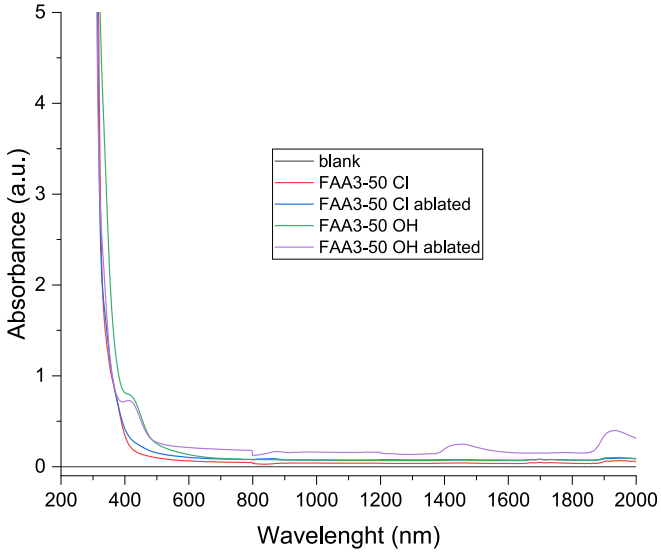

Fig. A.6. UV–Vis spectra comparison of ablated and not ablated membranes.

A.5 Contact pressure

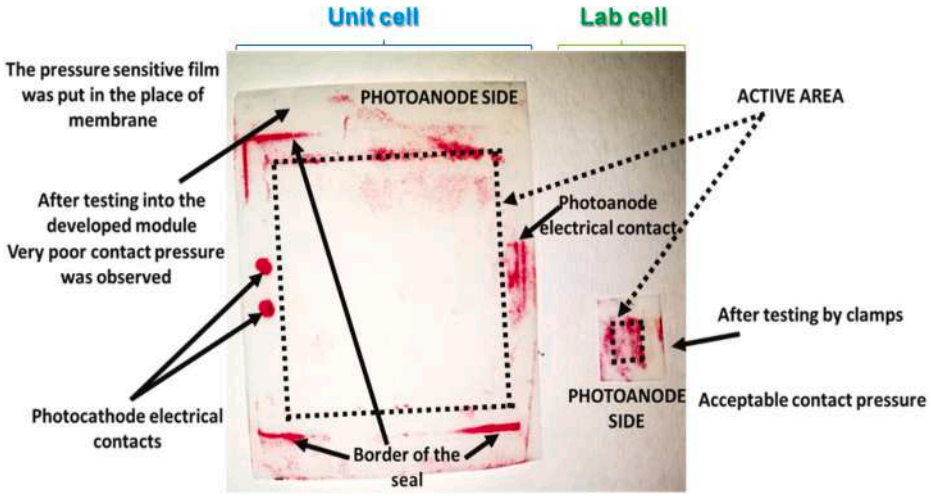

Fig. A.7. Contact pressure measurements, red-scale map of 25 cm^2 PEC cell (on the left) and 0.25 cm^2 lab cell (on the right).

References

[1] C. Acar, I. Dincer, Investigation of a novel photoelectrochemical hydrogen production system, Chem. Eng. Sci. 197 (2019) 74–86, https://doi.org/10.1016/j.ces.2018.12.014.

[2] P.K. Shukla, R.K. Karn, A.K. Singh, O.N. Srivastava, Studies on PV assisted PEC solar cells for hydrogen production through photoelectrolysis of water, Int. J. Hydrogen Energy 27 (2) (2002) 135–141, https://doi.org/10.1016/S0360-3199(01)00095-7.

[3] F.E. Osterloh, B.A. Parkinson, Recent developments in solar water-splitting photocatalysis, MRS Bull. 36 (1) (2011) 17–22, https://doi.org/10.1557/mrs.2010.5.

[4] M.K.H. Rabaia, et al., Environmental impacts of solar energy systems: a review, Sci. Total Environ. 754 (2021) 141989, https://doi.org/10.1016/j.scitotenv.2020.141989.

[5] A. Dhar, M.A. Naeth, P.D. Jennings, M. Gamal El-Din, Perspectives on environmental impacts and a land reclamation strategy for solar and wind energy systems, Sci. Total Environ. 718 (2020) 134602, https://doi.org/10.1016/j.scitotenv.2019.134602.

[6] M. Ahmed, I. Dincer, A review on photoelectrochemical hydrogen production systems: challenges and future directions, Int. J. Hydrogen Energy 44 (5) (2019) 2474–2507, https://doi.org/10.1016/j.ijhydene.2018.12.037.

[7] H. Narayanan, B. Viswanathan, K.R. Krishnamurthy, H. Nair, Hydrogen from Photo-Electrocatalytic Water Splitting, Elsevier Inc., 2019, https://doi.org/10.1016/B978-0-12-814853-2.00012-6.

[8] J.G. Mavroides, D.I. Tchernev, J.A. Kafalas, D.F. Kolesar, Photoelectrolysis of water in cells with TiO2 anodes, Mater. Res. Bull. 10 (10) (1975) 1023–1030, https://doi.org/10.1016/0025-5408(75)90210-X.

[9] P. Saravanan, M.R. Khan, C.S. Yee, D.V.N. Vo, An Overview of Water Electrolysis Technologies for the Production of Hydrogen, INC, 2020, https://doi.org/10.1016/B978-0-12-819553-6.00007-6.

[10] D. Ferrero, M. Santarelli, Investigation of a novel concept for hydrogen production by PEM water electrolysis integrated with multi-junction solar cells, Energy Convers. Manag. 148 (2017) (2017) 16–29, https://doi.org/10.1016/j.enconman.2017.05.059.

[11] P. Chatterjee, et al., Photovoltaic/photo-electrocatalysis integration for green hydrogen: a review, Energy Convers. Manag. 261 (April) (2022) 115648, https://doi.org/10.1016/j.enconman.2022.115648.

[12] T. Bak, J. Nowotny, M. Rekas, C.C. Sorrell, "Photo-electrochemical hydrogen generation from water using solar energy, Materials-related aspects," (2002) [Online]. Available: www.elsevier.com/locate/ijhydene.

[13] A. Carbone, M. Contreras, G. Roberto, A. Salvatore, Enhanced Photoelectrochemical Water Splitting at Hematite Photoanodes by E Ff Ect of a, 2020.

[14] V.M. Aroutiounian, V.M. Arakelyan, G.E. Shahnazaryan, Metal oxide photoelectrodes for hydrogen generation using solar radiation-driven water splitting, Sol. Energy 78 (5) (2005) 581–592, https://doi.org/10.1016/j.solener.2004.02.002.

[15] J. Juodkazyte, et al., Study on copper oxide stability in photoelectrochemical cell composed of nanostructured TiO2 and CuxO electrodes, Electrochim. Acta 137 (2014) 363–371, https://doi.org/10.1016/j.electacta.2014.05.140.

[16] C. Li, Z. Luo, T. Wang, J. Gong, in: Surface, Bulk, and Interface: Rational Design of Hematite Architecture toward Efficient Photo-Electrochemical Water Splitting," Advanced Materials, vol. 30, Wiley-VCH Verlag, Jul. 26, 2018, https://doi.org/10.1002/adma.201707502, 30.

[17] C. Du, J. Yang, J. Yang, Y. Zhao, R. Chen, B. Shan, An iron oxide -copper bismuth oxide photoelectrochemical cell for spontaneous water splitting, Int. J. Hydrogen Energy 43 (51) (Dec. 2018) 22807–22814, https://doi.org/10.1016/j.ijhydene.2018.10.170.

[18] X. Yang, C. Du, R. Liu, J. Xie, D. Wang, Balancing photovoltage generation and charge-transfer enhancement for catalyst-decorated photoelectrochemical water splitting: a case study of the hematite/MnOx combination, J. Catal. 304 (2013) 86–91, https://doi.org/10.1016/j.jcat.2013.04.014.

[19] D. Wang, Y. Chen, Y. Zhang, X. Zhang, N. Suzuki, C. Terashima, Boosting photoelectrochemical performance of hematite photoanode with TiO 2 underlayer by extremely rapid high temperature annealing, Appl. Surf. Sci. 422 (Nov. 2017) 913–920, https://doi.org/10.1016/j.apsusc.2017.05.164.

[20] X. Wang, et al., Efficient photo-electrochemical water splitting based on hematite nanorods doped with phosphorus, Appl. Catal. B Environ. 248 (Jul. 2019) 388–393, https://doi.org/10.1016/j.apcatb.2019.02.048.

[21] J. Kwon, et al., Photoreduction synthesis of hierarchical hematite/silver nanostructures for photoelectrochemical water splitting, Energy Technol. 4 (2) (Feb. 2016) 271–277, https://doi.org/10.1002/ente.201500221.

[22] F.P. Koffyberg, F.A. Benko, A photoelectrochemical determination of the position of the conduction and valence band edges of p-type CuO, J. Appl. Phys. 53 (2) (1982) 1173–1177, https://doi.org/10.1063/1.330567.

[23] M. Yin, et al., Copper oxide nanocrystals, J. Am. Chem. Soc. 127 (26) (2005) 9506–9511, https://doi.org/10.1021/ja050006u.

[24] C.Y. Chiang, Y. Shin, K. Aroh, S. Ehrman, Copper oxide photocathodes prepared by a solution based process, Int. J. Hydrogen Energy 37 (10) (2012) 8232–8239, https://doi.org/10.1016/j.ijhydene.2012.02.049.

[25] J. Han, X. Zong, X. Zhou, C. Li, Cu2O/CuO photocathode with improved stability for photoelectrochemical water reduction, RSC Adv. 5 (14) (2015) 10790–10794, https://doi.org/10.1039/c4ra13896a.

[26] K.H. Yoon, W.J. Choi, D.H. Kang, Photoelectrochemical properties of copper oxide thin films coated on an n-Si substrate, Thin Solid Films 372 (1) (2000) 250–256, https://doi.org/10.1016/S0040-6090(00)01058-0.

[27] K. Syrek, M. Jażdżewska, M. Kozieł, L. Zaraska, Photoelectrochemical activity of Cu2O electrochemically deposited at different temperatures, J. Ind. Eng. Chem. 115 (Nov. 2022) 561–569, https://doi.org/10.1016/j.jiec.2022.09.002.

[28] A.E. Rakhshani, Preparation, characteristics and photovoltaic properties of cuprous oxide-a review, Solid State Electron. 29 (1) (1986) 7–17, https://doi.org/10.1016/0038-1101(86)90191-7.

[29] Y.F. Lim, C.S. Chua, C.J.J. Lee, D. Chi, Sol-gel deposited Cu2O and CuO thin films for photocatalytic water splitting, Phys. Chem. Chem. Phys. 16 (47) (2014) 25928–25934, https://doi.org/10.1039/c4cp03241a.

[30] A. Paracchino, J.C. Brauer, J.E. Moser, E. Thimsen, M. Graetzel, Synthesis and characterization of high-photoactivity electrodeposited Cu 2O solar absorber by photoelectrochemistry and ultrafast spectroscopy, J. Phys. Chem. C 116 (13) (2012) 7341–7350, https://doi.org/10.1021/jp301176y.

[31] A. Vilanova, T. Lopes, A. Mendes, Large-area photoelectrochemical water splitting using a multi-photoelectrode approach, J. Power Sources 398 (May) (2018) 224–232, https://doi.org/10.1016/j.jpowsour.2018.07.054.

[32] A. Vilanova, T. Lopes, C. Spenke, M. Wullenkord, A. Mendes, Optimized photoelectrochemical tandem cell for solar water splitting, Energy Storage Mater. 13 (Jul. 2018) 175–188, https://doi.org/10.1016/j.ensm.2017.12.017.

[33] A. Landman, et al., Decoupled photoelectrochemical water splitting system for centralized hydrogen production, Joule 4 (2) (2020) 448–471, https://doi.org/10.1016/j.joule.2019.12.006.
[34] M. Boschetti, et al., Modular stand-alone photoelectrocatalytic reactor for emergent contaminant degradation via solar radiation, Sol. Energy 228 (August) (2021) 120–127, https://doi.org/10.1016/j.solener.2021.09.027.
[35] S. Ghosh, I. Dincer, Development and analysis of a new light-based hydrogen production system, Int. J. Hydrogen Energy 41 (19) (2016) 7976–7986, https://doi.org/10.1016/j.ijhydene.2015.11.151.
[36] G.C. Tedesco, P.B. Moraes, Innovative design of a continuous flow photoelectrochemical reactor: hydraulic design, CFD simulation and prototyping, J. Environ. Chem. Eng. 9 (5) (2021) 105917, https://doi.org/10.1016/j.jece.2021.105917.
[37] C. Carver, Z. Ulissi, C.K. Ong, S. Dennison, G.H. Kelsall, K. Hellgardt, Modelling and development of photoelectrochemical reactor for H 2 production, Int. J. Hydrogen Energy 37 (3) (2012) 2911–2923, https://doi.org/10.1016/j.ijhydene.2011.07.012.
[38] N.A. Kelly, T.L. Gibson, Solar energy concentrating reactors for hydrogen production by photoelectrochemical water splitting, Int. J. Hydrogen Energy 33 (22) (2008) 6420–6431, https://doi.org/10.1016/j.ijhydene.2008.08.015.
[39] G. Giacoppo, et al., 1.5 kWe HT-PEFC stack with composite MEA for CHP application, Int. J. Hydrogen Energy 38 (26) (2013) 11619–11627, https://doi.org/10.1016/j.ijhydene.2013.04.044.
[40] P. Dzik, M. Veselý, M. Králová, M. Neumann-Spallart, Ink-jet printed planar electrochemical cells, Appl. Catal. B Environ. 178 (2015) 186–191, https://doi.org/10.1016/j.apcatb.2014.09.030.
[41] K. Fujii, K. Ohkawa, Hydrogen generation from aqueous water using n-GaN by photoassisted electrolysis, Phys. Status Solidi Curr. Top. Solid State Phys. 3 (6) (2006) 2270–2273, https://doi.org/10.1002/pssc.200565171.
[42] T. Lopes, P. Dias, L. Andrade, A. Mendes, An innovative photoelectrochemical lab device for solar water splitting, Sol. Energy Mater. Sol. Cells 128 (Sep. 2014) 399–410, https://doi.org/10.1016/j.solmat.2014.05.051.
[43] K. Brinkert, et al., Efficient solar hydrogen generation in microgravity environment, Nat. Commun. 9 (1) (Dec. 2018), https://doi.org/10.1038/s41467-018-04844-y.
[44] J. Hogerwaard, I. Dincer, G.F. Naterer, Experimental investigation and optimization of integrated photovoltaic and photoelectrochemical hydrogen generation, Energy Convers. Manag. 207 (January) (2020) 112541, https://doi.org/10.1016/j.enconman.2020.112541.
[45] A.M.M.I. Qureshy, I. Dincer, Development of a new solar photoelectrochemical reactor design for more efficient hydrogen production, Energy Convers. Manag. 228 (December 2020) (2021) 113714, https://doi.org/10.1016/j.enconman.2020.113714.
[46] D. Kumar, A.K. Gautam, N. Khare, Thermoelectric voltage triggered self-biased photoelectrochemical water splitting utilizing visible light active Ag/NaNbO3 nanocomposite photoanode, Energy Convers. Manag. 277 (September 2022) (2023) 116632, https://doi.org/10.1016/j.enconman.2022.116632.
[47] K. Aryal, B.N. Pantha, J. Li, J.Y. Lin, H.X. Jiang, Hydrogen generation by solar water splitting using p-InGaN photoelectrochemical cells, Appl. Phys. Lett. 96 (5) (2010) 2008–2011, https://doi.org/10.1063/1.3304786.
[48] P.N. Ciesielski, et al., Photosystem I - based biohybrid photoelectrochemical cells, Bioresour. Technol. 101 (9) (2010) 3047–3053, https://doi.org/10.1016/j.biortech.2009.12.045.
[49] S. Trocino, et al., Dry hydrogen production in a tandem critical raw material-free water photoelectrolysis cell using a hydrophobic gas-diffusion backing layer, Catalysts 10 (11) (2020) 1–23, https://doi.org/10.3390/catal10111319.
[50] C. Lo Vecchio, et al., Water splitting with enhanced efficiency using a nickel-based co-catalyst at a cupric oxide photocathode, Catalysts 11 (11) (2021) 1–11, https://doi.org/10.3390/catal11111363.
[51] C. Lo Vecchio, et al., Anionic exchange membrane for photo-electrolysis application, Polymers 12 (12) (2020) 1–12, https://doi.org/10.3390/polym12122991.
[52] Y.K. Hsieh, et al., Direct micromachining of microfluidic channels on biodegradable materials using laser ablation, Polymers 9 (7) (2017), https://doi.org/10.3390/polym9070242.
[53] A. Carbone, S.C. Zignani, I. Gatto, S. Trocino, A.S. Aricò, Assessment of the FAA3-50 polymer electrolyte in combination with a NiMn2O4 anode catalyst for anion exchange membrane water electrolysis, Int. J. Hydrogen Energy 45 (16) (2020) 9285–9292, https://doi.org/10.1016/j.ijhydene.2020.01.150.
[54] G. Giacoppo, et al., Numerical 3D model of a novel photoelectrolysis tandem cell with solid electrolyte for green hydrogen production, Energies 16 (4) (2023) 1–12, https://doi.org/10.3390/en16041953.